Hindawi
Shock and Vibration
Volume 2021, Article ID 9962519, 15 pages
https://doi.org/10.1155/2021/9962519

Research Article

Numerical Simulation of Characteristics of Wind Field at Bridge Sites in Flat and Gorge Terrains under the Thunderstorm Downburst

Peng Hu, Yilin Chen, Yan Han, Fei Zhang, and Yongjian Tang

School of Civil Engineering, Changsha University of Science & Technology, Changsha, Hunan 410114, China

Correspondence should be addressed to Yan Han; ce_hanyan@163.com

Received 4 April 2021; Accepted 16 July 2021; Published 26 July 2021

Academic Editor: Roberto Nascimbene

To investigate the effects of thunderstorm downburst on the characteristics of wind field at bridge sites in flat and gorge terrains, firstly, numerical simulation of wind fields in the flat terrain under the thunderstorm downburst was conducted through the SST k-ω turbulence model, combined with the impinging jet technology. After verification of the reliability of the numerical model, settings, and methods, the characteristics of wind field over a long-span bridge site in a gorge terrain under the thunderstorm downburst were investigated and the distributions of wind speed and wind attack angle in the flat and gorge terrains were compared. The results show that, under the effects of the thunderstorm downburst, the wind speeds are relatively maximum at the midspan point of the girder in the flat terrain. Besides, the farther away from the midspan point, the smaller the wind speeds, which is opposite to the case in the gorge terrain. The wind speeds at each typical monitoring point are basically the same in the two terrains, before the thunderstorm downburst hits the bridge girder. Later the wind speeds at each point in the gorge terrain are much higher than those in the flat terrain. Most wind attack angles are negative at the monitoring points in the flat terrain, but the farther away they are from the midspan point, the greater the wind attack angles will be. However, the wind attack angles at the monitoring points in the gorge terrain are generally larger than those in the flat terrain, and they gradually turn to be positive farther away from the midspan point. In the flat terrain, both wind speeds and wind attack angles (or their absolute values) at the girder are large within about $t = 75$~130 s, indicating that the thunderstorm downburst may exert significant effects on the bridge. However, in the gorge terrain, due to the large wind speeds and wind attack angles (or their absolute values) at the girder after $t = 75$ s, full attention needs to be paid to the effects of the thunderstorm downburst during this period.

1. Introduction

Thunderstorm downbursts are strong vertically downward winds caused by the confrontation of cold and warm flow in the sky, which spread around after hitting the ground, thus forming very high strong wind fields near the ground. It is reported that the maximum instantaneous wind speed near the ground can reach 67 m/s under thunderstorm downbursts [1, 2]. According to the analysis of relevant data, Proctor [3] reported that the thunderstorm downburst is a common type of weather phenomenon, with the probability of occurrence reaching as high as 60%~70% in strong convective weather, which has caused damage to a large number of engineering structures all over the world. Due to the frequent occurrence of thunderstorm downbursts, the design control loads of wind-resistant for structures in most areas of Europe and the United States were determined by thunderstorm downbursts. Generally, the research on the effects of thunderstorm downbursts on the structures has become a hot issue in the field of wind engineering in recent years [4, 5].

Over the last 50 years, a large quantity of research has been conducted to better understand the formation and movement mechanism of thunderstorm downbursts and finally to conduct predictability analysis, including field measurements, wind tunnel tests, and numerical simulations. Fujita [6] provides large area mapping of thunderstorm downbursts by using the measurement data at meteorological stations in the United States in 1978. Wakimoto [7] investigated the time-varying characteristics

of thunderstorm downbursts based on the data of NIMROD project in 1982 and divided the thunderstorm downbursts into four stages as follows: (a) the formative stage; (b) the early mature stage; (c) the late mature stage; and (d) the dissipation stage. In 1990, Fujita [1] divided thunderstorm downbursts into microburst winds and macroburst winds according to the level of materiality. The affected region of the former type is smaller than 4 km, while that of the latter is greater than 4 km. By sorting out the wind field data of thunderstorm downbursts observed in Colorado, USA, Hjelmfelt [8] studied the symmetry and the spatial distribution characteristics of wind field parameters caused by the thunderstorm downbursts. Zhang et al. [9] systematically analyzed the data of thunderstorm downbursts recorded by 9 anemometers installed at different heights in a high meteorological tower, and the characteristics of a wide dataset of thunderstorm downburst signals were analyzed in a statistical environment. Although field measurement is probably the most reliable method to study thunderstorm downbursts, it is hard to achieve since it requires mature technology and enormous economic costs. Above all, the short duration and uncertainty in space and time of thunderstorm downbursts greatly increase the difficulties in observations and measurements. Therefore, thunderstorm downbursts were often studied by wind tunnel tests and numerical simulations.

Regarding wind tunnel tests and numerical simulations, Wood et al. [10] developed a test device to simulate the wind fields of steady thunderstorm downbursts, the radial position of the maximum wind speed was determined, the wind profile of each position was obtained, and the original theoretical model was improved according to the test results. Lin and Savory [11] simulated thunderstorm downbursts by using the impinging jet technology, and part of the characteristics of thunderstorm downbursts were approximately simulated. Chay and Letchford [12] better simulated the three-dimensional wind fields of the thunderstorm downburst through a wall jet model. Li et al. [13] carried out numerical simulations on stationary thunderstorm downbursts and established a simple empirical model for vertical and radial shaping of the horizontal wind speeds. Chen and Letchford [14] built an empirical numerical model for downburst wind fields according to a nonparametric deterministic-stochastic hybrid method based on two sets of full-scale wind speed records from thunderstorm downbursts. Liu et al. [15] studied the thunderstorm downbursts through setting an inclined plate both in a computational domain and an atmospheric boundary layer wind tunnel. The corresponding numerical simulation results were in good agreement with the wind tunnel test results, and these indicated that the characteristics of stationary thunderstorm downbursts could be reasonably simulated by setting an inclined plate in a boundary layer wind tunnel. The research above has achieved abundant conclusions and results for better understanding the characteristics of thunderstorm downbursts through field measurements, wind tunnel tests, and numerical simulations. However, it should be noted that most studies above just concentrated on the thunderstorm downbursts over flat terrain. With the continuously deepening understanding of thunderstorm downbursts, it is found that thunderstorm downbursts also occur frequently in complex mountainous and show different wind field characteristics.

Aiming at the wind field characteristics of thunderstorm downburst in complex mountain terrains, Mason et al. [16] studied the structures of thunderstorm downbursts in mountain terrains through numerical simulation and found that the maximum wind speed caused by thunderstorm downbursts in the mountain terrain is more than 30% higher than that in the flat terrain. Abd-Elaal et al. [17] studied the changes of horizontal and vertical wind speeds during the thunderstorm downburst in two real complex terrains. It is found that the longitudinal width of mountainous or hills can affect the wind fields significantly, which can strengthen the vertical downward wind speeds and generate effective wind velocity components on low-altitude inclined surfaces. Huang et al. [18] found that thunderstorm downbursts occur more frequently in mountain terrains through field measurements, which raises new questions in wind-resistance design of long-span bridges located in mountain and gorge terrains. The research above shows that complex terrains can strengthen the wind speeds during a thunderstorm downburst and make the thunderstorm downburst more frequent, which will greatly enhance the destructiveness of thunderstorm downbursts. For example, in March 2013, the Chishi Bridge located in a complex terrain in Hunan Province was hit by a sudden thunderstorm downburst, which damaged the temporary facilities of the bridge, with an instantaneous wind speed of 32.0 m/s. In May 2016, the Balinghe Bridge straddling a gorge terrain was also suddenly hit by a thunderstorm downburst, with an instantaneous wind speed of 32.7 m/s. This thunderstorm downburst results in the damage of dozens of lamps, some communication optical cables, and cable pipelines. Besides, the traffic was stopped for nearly 5 hours. The facts above show that thunderstorm downbursts have great effects on bridges in mountainous areas, which needs to be paid enough attention. On the other hand, with the increasing number of long-span bridges built in mountainous areas, these bridges shall inevitably straddle gorge terrains. However, there is a lack of relevant research currently. Most existing wind-resistance specifications or criteria fail to include complex wind types such as thunderstorm downbursts, without corresponding provisions for the wind loads caused by thunderstorm downbursts for designing [19]. Therefore, studies on the wind field characteristics under thunderstorm downbursts in complex terrains are of great significance for the wind field characteristics of long-span bridges located in mountainous areas and their wind-resistance designs.

Aiming at the problems above, the effects of the thunderstorm downburst on the characteristics of wind field at the bridge sites in flat and gorge terrains were investigated in this paper. Firstly, the wind fields of the thunderstorm downburst in the flat terrain are verified. After verification of the reliability of the numerical model, settings, and methods, a numerical simulation is conducted on the wind field characteristics in gorge terrain under the thunderstorm downburst, and the distributions of wind speeds and wind

attack angles at the midspan point, 1/4 span point, and bridge tower in the flat and gorge terrains are analyzed. Finally, some main conclusions are concluded.

2. Establishment and Verification of the Numerical Model of Thunderstorm Downbursts

In order to verify the accuracy and reliability of the numerical model of thunderstorm downbursts, the wind fields of the stationary thunderstorm downburst in the flat terrain were simulated, and the calculated results were compared with the existing research data.

2.1. Establishment and Verification of the Wind Field in the Flat Terrain. A three-dimensional computational domain was used for simulation, with reference to the actual dimensions of thunderstorm downbursts [17]. The size of computational domain was determined as $11D_{jet} \times 11D_{jet} \times 4D_{jet}$, where $1D_{jet} = 1000$ m, representing the diameter of the jet outlet. According to the research by Hao and Wu [20], the height of the nozzle from the ground was set as $2D_{jet}$. From the research by Mason et al. [21], the SST k-ω turbulence model can achieve more accurate results in impinging jet simulation, which thus was adopted in this paper. During calculation, the pressure-velocity coupling algorithm was solved by SIMPLEC algorithm, and the pressure, momentum, turbulent kinetic energy, dissipation rate of turbulent kinetic energy, and Reynolds stress were all discretized by the second-order scheme, with the residual values set as $10e-6$. In terms of boundary conditions, when defining the inlet boundary condition in the traditional atmospheric boundary layer, the profiles of mean wind speed and turbulent wind speed should be set at the inlet, which is a difficult issue to be carefully considered [22]. Furthermore, for the complex terrains, the inlet boundary condition will be more complicated. However, for modeling the thunderstorm downbursts by using the impinging jet simulation method, only the jet velocity should be defined for the nozzle. In other words, the inlet boundary condition of the thunderstorm downburst is relatively simpler than that of the traditional atmospheric boundary layer. More specifically, when modeling the thunderstorm downbursts in the flat terrain, gorge terrain, and other complex terrains, the nozzles are set as the inlet boundary condition with only defining a jet velocity. In the present study, the jet velocity at the nozzle was set as 40 m/s [20], while the wall boundary condition was applied for the ground, and the pressure-outlet boundary condition was used for the top and sides. Transient calculation was adopted in this paper, with the time step of 0.005 s, and the total calculation time of about 250 s. With regard to the mesh scheme of the computational domain, structured grid was adopted in the whole computational domain, and the O-type grid was used to ensure the smooth transition of the mesh near the nozzle. Before conducting the calculation, three different mesh schemes were generated for independence test. The mesh scheme 1 has 1.29 million cells, the mesh scheme 2 has 1.10 million cells, and scheme 3 has 0.83 million cells. The first layer heights for three mesh schemes are $5e-6D_{jet}$, $1e-5D_{jet}$ and $5e-5D_{jet}$, respectively, and they are fine enough for full-scale models. The radial and vertical growth rates for mesh scheme 1, mesh scheme 2, and mesh scheme 3 are about 1.12, 1.14, and 1.16, respectively. The mesh scheme 1 and the computational domain for the flat terrain are shown in Figure 1.

After the thunderstorm downburst in flat terrain reaches a stable state, its average wind field can be calculated based on the settings above, in which the radial and vertical profiles of horizontal wind speed calculated with different mesh schemes were compared with previous studies [8, 13, 14, 16], as shown in Figure 2. In this figure, the height of the radial profile is taken as $z = 0.05D_{jet}$, and the distance between the vertical profile and the center of thunderstorm downburst is $r = 1.5D_{jet}$, where u is the horizontal wind speed, u_{max} represents the maximum horizontal wind speed, z_{max} is the vertical height corresponding to the maximum horizontal wind speed, and r_{umax} refers to the radial distance corresponding to the maximum horizontal wind speed. On the one hand, the results of normalized radial and vertical profiles of horizontal wind speed with different mesh schemes are close to each other, indicating approximate independence of the simulation results on these mesh schemes. On the other hand, the present numerical results are also very consistent with the previous studies, validating the rationality and feasibility of the present numerical model, mesh scheme, and other settings. It should be noted that the numerical results obtained from mesh scheme 1 are relatively closer to the previous studies, so mesh scheme 1 is used for further numerical simulation research, as shown in Figure 2.

More importantly, the characteristics of thunderstorm downbursts are quite different from those of traditional wind characteristics in the atmospheric boundary layer. As is well known, for the traditional wind fields in atmospheric boundary layer, the horizontal wind speeds are equal at the same height, and they increase exponentially or logarithmically with the increase of heights from the ground. In contrast, in thunderstorm downbursts, the horizontal wind speeds gradually increase along the radial distance and then gradually decrease with the increase of the radial distance, as shown in Figure 2(a). Meanwhile, in the vertical profile of the horizontal wind speed, the wind speed reaches its maximum near the ground and then decreases with the increase of heights from the ground, as shown in Figure 2(b).

2.2. Establishment of the Numerical Model for the Gorge Terrain. As mentioned above, the gorge terrain is the most commonly found in the bridge site of long-span bridges in mountainous areas. Therefore, the corresponding numerical model for the gorge terrain was established according to the actual long-span bridge and the gorge terrain in the bridge site, as shown in Figure 3. The gorge terrain is simplified as a "V" shape with an included angle of 120°. Its length is consistent with the length of the computational domain, with the width of 1196 m and the height of 345.3 m. The

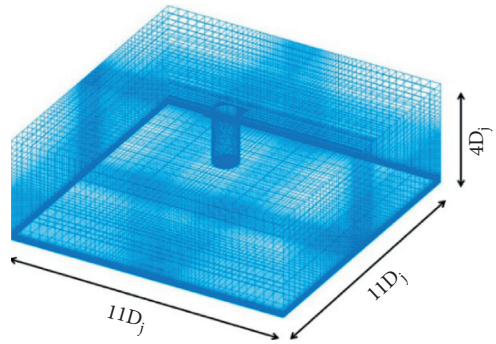

Figure 1: Mesh scheme 1 and the computational domain for the flat terrain.

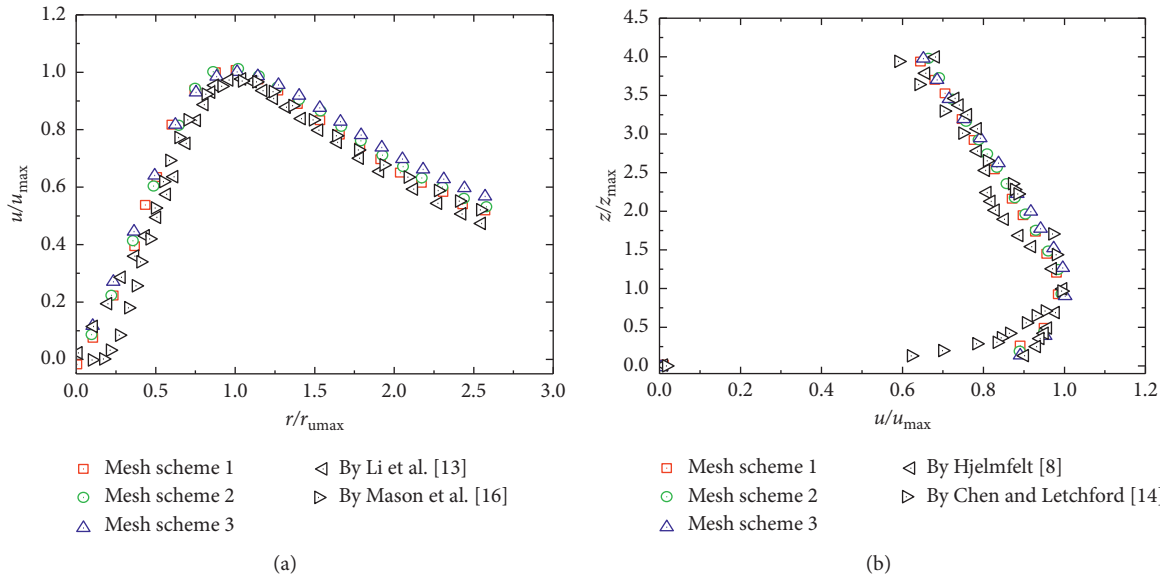

Figure 2: Comparisons of (a) radial and (b) vertical profiles of horizontal wind speed.

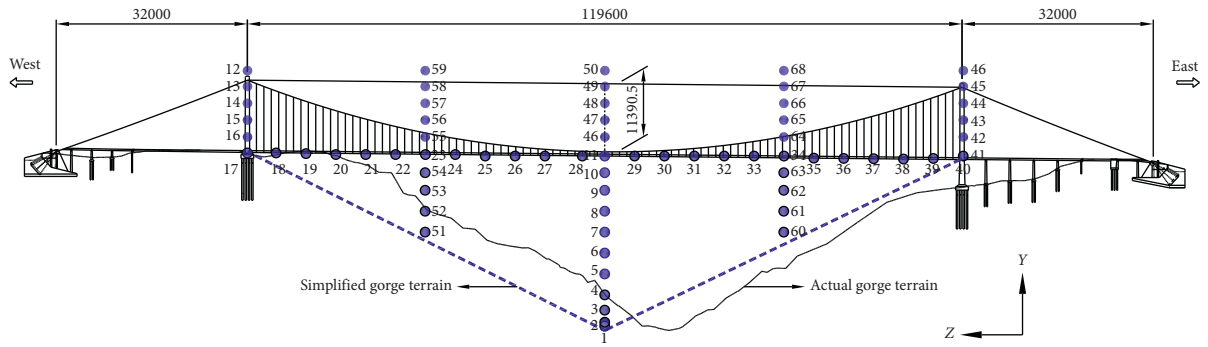

Figure 3: Bridge site and the monitoring points (unit: cm).

lowest point of the gorge terrain is as high as that of the flat terrain. Other settings, such as the size of the computational domain, boundary conditions, and mesh scheme, are consistent with those of the flat terrain as much as possible. The final mesh scheme of the gorge terrain under the thunderstorm downburst is shown in Figure 4. According to the actual bridge layout, the long-span bridge straddles the top of the gorge, the main span length is 1196 m, consistent with the width of the gorge, and the bridge towers are located on both sides of the gorge. In order to facilitate subsequent data extraction, a total of 68 monitoring points were set in the computational domain, as shown in Figure 3. Specifically, the intervals of monitoring points set along the bridge girder are about 50 m, and the intervals of monitoring points

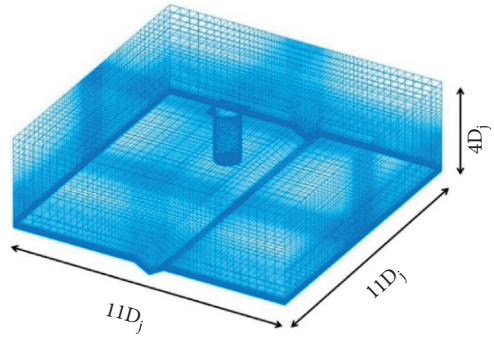

Figure 4: Overall mesh for the gorge terrain.

set along the 1/4 span line, 3/4 span line, midspan line, and the bridge towers are about 40 m, where point 1 is 4.9 m above the ground and point 11 is at the midspan point of the girder. Since the wind speeds will reach their maximum values when their horizontal distances to the center point of the nozzle are about $1.0D_{jet}$, this typical position was chosen for analyzing the wind field characteristics at the bridge site. Meanwhile, for the sake of comparing the differences between the characteristics of wind fields at the bridge site under thunderstorm downbursts in gorge terrain and those in flat terrain, the same monitoring points were set at the same positions in the numerical model of the flat terrain. After calculation, the wind speed and wind attack angle of each monitoring point could be obtained.

3. Analysis on Wind Fields over the Bridge Sites under the Thunderstorm Downburst

In order to study the effects of thunderstorm downburst on the wind fields over the bridge sites of long-span bridge in flat terrain and gorge terrains, the time-history curves of wind speed and wind attack angle of each monitoring point at the girder and bridge towers are extracted from the beginning of the thunderstorm downburst occurring, and the wind fields caused by different terrains are compared and analyzed.

3.1. Distributions of Horizontal Wind Speed at the Bridge Site

3.1.1. Distributions of Horizontal Wind Speed at the Girder. Figures 5 and 6 show the typical time-history curves of horizontal wind speed at the midspan ($z = 0$ m), 1/4 span point ($z = \pm 300$ m), and 1/8 span point ($z = \pm 150$ m, ± 450 m) of the bridge girder in flat terrain and gorge terrains, respectively. It can be seen that the time-history curve of wind speed at the left 1/4 span or 1/8 span point is consistent with that of the corresponding point on the right side, which verifies the axisymmetry of thunderstorm downburst wind field [8]. The comparison between Figures 5 and 6 shows that the wind speeds are relatively maximum at the midspan point of the girder in flat terrain, and the farther away from the midspan point, the smaller the time-history values of wind speeds. However, the wind speeds are relatively minimum at the midspan point of the girder in gorge terrain,

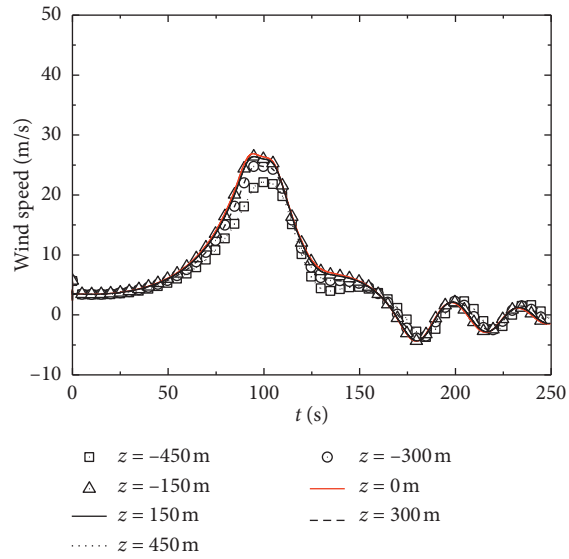

Figure 5: Time-history curves of horizontal wind speed in the flat terrain.

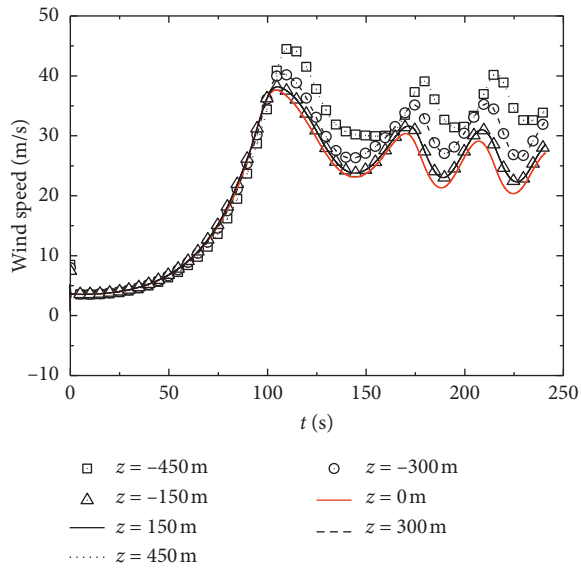

Figure 6: Time-history curves of horizontal wind speed in the gorge terrain.

and the farther away from the midspan point, the larger the time-history values of wind speeds. In addition, with regard to the variation trend of wind speed in the flat terrain, the wind speed at each typical monitoring point increases rapidly with the passage of time before 100 s, which reflects the thunderstorm downburst gradually reaching the monitoring points. During the period from 100 s to 175 s, the wind speed at each point basically decreases gradually with the occurrence of reverse speed (the wind speed is below zero). After 175 s, the wind speed at each point fluctuates to some extent with the passage of time. For the gorge terrain, the variation trend of wind speed measured at each monitoring point is similar to that in the flat terrain. Although the wind speed at each point in the gorge terrain also

gradually decreases from 100 s to 150 s, the difference lies in that the wind speeds are all above zero without reverse speeds, indicating that the wind fields in the gorge are quite different from those in the flat terrain due to the effects of gorge terrain.

Since the wind field over the bridge site is symmetrical by the midspan line, the wind speeds at monitoring points in the left span could be further compared. Figure 7 shows the comparisons of time-history curve of wind speed at several typical monitoring points in the left span between the flat terrain and the gorge terrain. It can be seen that, before about 92 s, namely, before the thunderstorm downburst hits the bridge site, the wind speeds at each typical monitoring point are basically the same in the two terrains. Afterwards, the wind speeds at each point over the gorge terrain are much higher than those in the flat terrain. Meanwhile, it can be observed that the peak of wind speed in the gorge terrain occurs later than that in the flat terrain. These phenomena indicate that the wind speeds at each monitoring point in the gorge terrain have been significantly strengthened, with lags in wind speed due to the effects of gorge terrain.

To illustrate the differences between the wind fields in flat and gorge terrains under the thunderstorm downburst, the streamlines and contour of wind speed in the two terrains at different typical time are given in Figure 8, where the red circle represents the position of the bridge girder. As shown in the figure, when $t = 50$ s, the thunderstorm downburst is in the sinking stage but has not hit the ground. Due to the drag and entrainment between downward flow and the surrounding flow, symmetrical vortexes are formed on both sides of the downward flow, and the wind fields in flat terrain are basically the same as those in the gorge terrain. When $t = 100$ s, the thunderstorm downburst starts to hit the bridge girder, and the main vortex in the flat terrain has reached the height of the bridge, while that in the gorge terrain has not reached the bridge yet. In other words, the main vortex in the gorge terrain is higher than that in the flat terrain. Since the wind speeds in the region of main vortex tend to weaken, the wind speeds in flat terrain are smaller than those in the gorge terrain at this time. On the other hand, the thunderstorm downburst spreads around after hitting the ground. The flow can spread in all directions in flat terrain, while it only spreads forward and backward in the gorge terrain. Due to the extrusion of the gorge terrain on the flow, the wind speeds in gorge terrain are higher than those in the flat terrain, as shown in Figure 7. After a period of time (about 10 s), the main vortex in the gorge terrain also reaches the height of the girder, and the wind speeds around the girder in the gorge terrain also start to decrease at this moment, which is shown as the maximum wind speed in the gorge terrain lagging behind that in the flat terrain in Figure 7. When $t = 150$ s, the downward flow has hit the ground and spread around. The main vortex continues to move downward, but due to the obstruction of terrain, it also gradually starts to move horizontally, which exerts more significant effects on the girder at this moment. As shown in Figure 7, the wind speeds in the two terrains are obviously reduced compared with those of $t = 100$ s. When $t = 180$ s, as the flow continues to move and spread around, the wind speeds around the girder gradually decrease, and a second vortex appears, which almost approaches the girder and directly affects it in the flat terrain, corresponding to negative values of wind speed around the girder in Figure 7. However, there remains certain distance between the vortex and the girder in the gorge terrain. At this time, the wind speeds around the girder are relatively less affected by the vortex, so the wind speeds in gorge terrain still maintain a relatively higher level. Subsequently, when $t = 210$ s~240 s, a third vortex appears in the two terrains. The height of the first vortex in gorge terrain is getting higher and higher because the flow is lifted by the slopes on both sides of the gorge terrain. Meanwhile, the heights of three vortexes in the flat terrain are basically equal. Overall, on the one hand, the distances between the vortexes and the girder in the gorge terrain are always larger than those in the flat terrain after $t = 100$ s, so the vortexes exert fewer effects on the wind fields around the girder in the gorge terrain and finally enable the wind speeds around the girder in the gorge terrain to be always greater than those in the flat terrain. On the other hand, as the downward flow reaches the ground and spreads around, the wind speeds in the two terrains fluctuate with the occurrence and dissipation of vortexes. The difference is that the wind speeds in the gorge terrain fluctuate in the range of high wind speed, while those in the flat terrain fluctuate near zero value.

As shown in the analysis above, $t = 50$ s, $t = 100$ s, and $t = 150$ s approximately correspond to the sinking stage of thunderstorm downburst, the stage of reaching or are about to reach the height of the girder, and the stage of hitting the ground and spreading around, respectively. Therefore, Figure 9 further shows the contour of wind speeds in the cross section of flat and gorge terrains at the three typical time above. It can be observed that when $t = 50$ s, the wind speeds in flat and gorge terrains are in lighter color, indicating that the two terrains are in low wind speeds. When the thunderstorm downburst begins to hit the girder at $t = 100$ s, the midspan point in flat terrain is in yellow color, while the both sides are in green color. However, the midspan point in gorge terrain is in yellow color, with dark yellow color of the two sides. Corresponding to Figures 5 and 6, the wind speeds at midspan point are high, while those of the both sides are small in flat terrain. In contrast, the wind speeds at midspan point are small in gorge terrain, with high speeds of the two sides. When the thunderstorm downburst hits the ground and spreads around at $t = 150$ s, the wind speeds at the height of the girder decrease in the two terrains, but the relationship between the wind speeds at the midspan point and the two sides is similar to those at $t = 100$ s, as shown in Figures 5 and 6.

3.1.2. Distributions of Vertical Profile of the Horizontal Wind Speed. For the three typical times of $t = 50$ s, $t = 100$ s, and $t = 150$ s, the distributions of vertical profile of the horizontal wind speed at the midspan point, 3/4 span point, and the left bridge tower in flat and gorge terrains are shown in Figure 10. Overall, the distributions of wind speed profiles in flat and gorge terrains are far different from those of logarithmic law or exponential law in traditional atmospheric

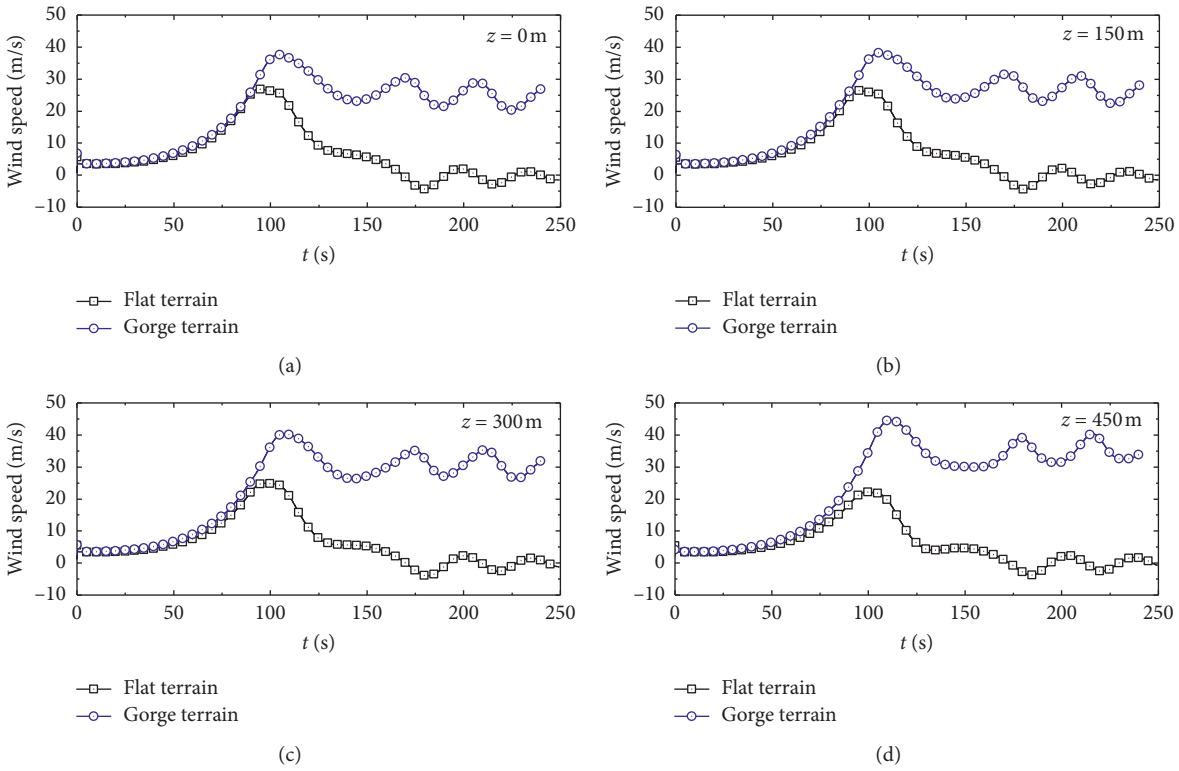

Figure 7: Comparisons of time-history curve of wind speed between the flat terrain and the gorge terrain.

boundary layer. Specifically, when $t = 50$ s, the lower the heights from the ground, the smaller the wind speeds in the two terrains. With the increase of heights from the ground, the wind speeds gradually increase with a very small amplitude. When $t = 100$ s, the wind speeds at the midspan and 3/4 span points in the two terrains increase at first and then gradually decrease with the increase of heights from the ground. It should be noted that the wind speed at the 40 m above the bridge girder is the maximum in the gorge terrain, while the maximum wind speed is found at 120 m below the bridge girder in the flat terrain. The reason is related to the relative position between the main vortex and the girder, based on the analysis of Figure 8. Meanwhile, it is also shown in Figure 9 that the position with the maximum wind speed in gorge terrain is higher than that in flat terrain. When $t = 150$ s, the wind speeds at the midspan and 3/4 span points below the girder in the gorge terrain vary slightly, but they rapidly decrease above the girder. With respect to the flat terrain, the wind speeds at these typical points generally decrease rapidly with heights from the ground.

3.2. Distributions of Wind Attack Angle at the Bridge Site

3.2.1. Distributions of Wind Attack Angle at the Girder. The time-history curves of wind attack angle at typical monitoring points on the left side of the midspan point under the thunderstorm downburst in the flat terrain are shown in Figure 11. Generally, most wind attack angles at measuring points are negative, but the farther away from the midspan point, the larger the wind attack angles. Specifically, the values of wind attack angle at typical monitoring points gradually increase from negative to positive before 100 s, which reflects the downward flow begins to reach the bridge girder (as shown in Figure 8). However, when $t = 100$ s~125 s, the wind attack angles at each typical monitoring point gradually decrease to be negative. Meanwhile, it is noted that, before 125 s, the closer the measuring point is to the midspan point, the smaller the fluctuation amplitude is. Hereafter, the fluctuation amplitude of the wind attack angles at each measuring point increases rapidly, with the maximum value approaching 90° and the minimum value approaching −90°. Figure 12 shows the time-history curves of wind attack angle at the corresponding typical monitoring points on the left side of the midspan point in gorge terrain. Overall, the variation trend of wind attack angles at each typical monitoring point in the gorge terrain is similar to that in flat terrain. However, the wind attack angles at the monitoring points farther away from the midspan point gradually turn to be positive. For instance, the wind attack angle at the monitoring point 500 m away from the midspan point is basically positive. Besides, the comparison between Figures 11 and 12 indicates that the wind attack angles measured at the typical points in gorge terrain are generally larger than those in flat terrain, with a much smaller fluctuation range.

Figure 13 shows the comparisons between the time-history curves of wind attack angle at each typical monitoring point in the flat and gorge terrains. It can be seen that when the thunderstorm downburst hits the bridge girder

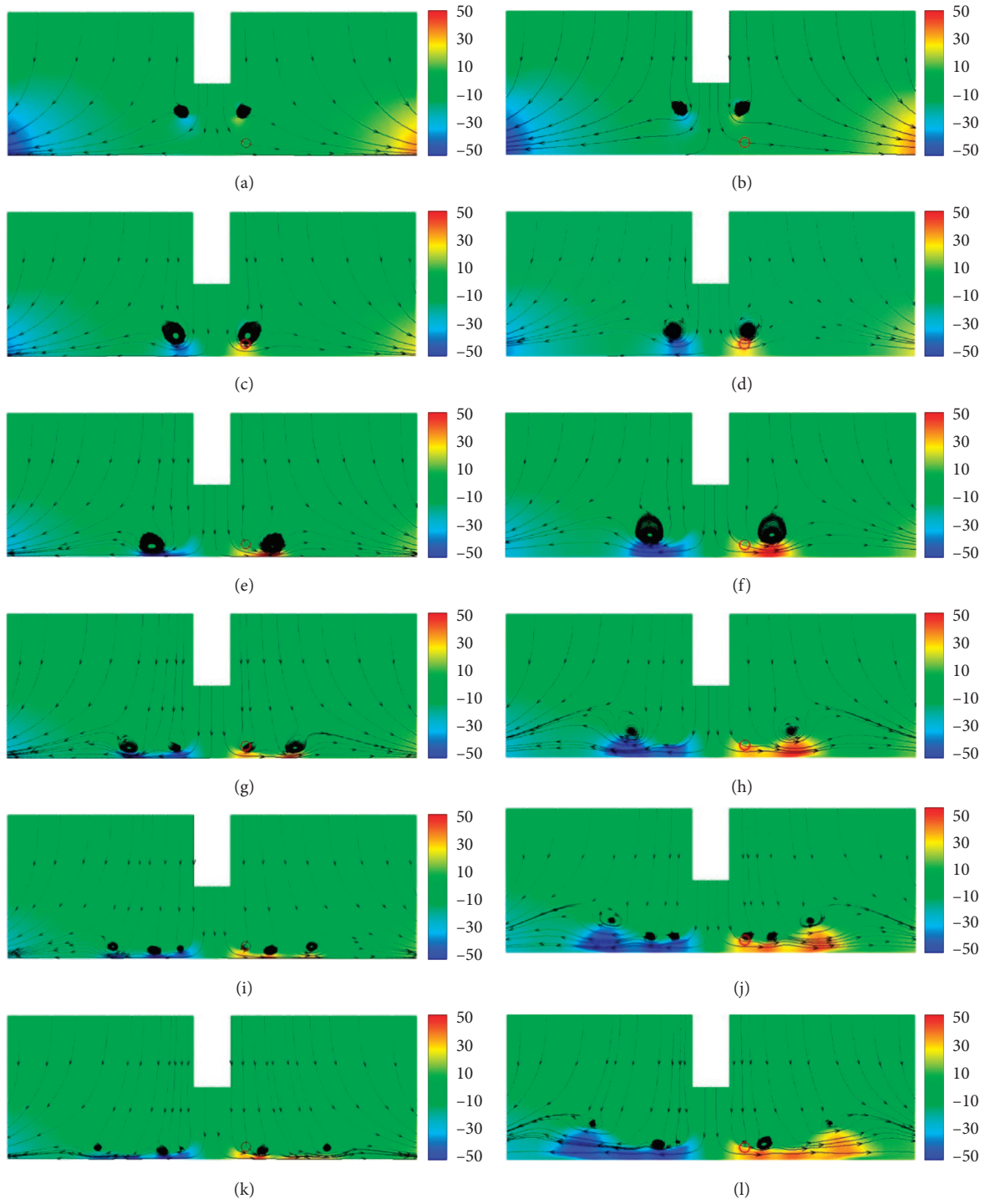

Figure 8: Streamlines and contour of wind speed in the flat and gorge terrains at different typical time. (a) Flat terrain, $t = 50$ s. (b) Gorge terrain, $t = 50$ s. (c) Flat terrain, $t = 100$ s. (d) Gorge terrain, $t = 100$ s. (e) Flat terrain, $t = 150$ s. (f) Gorge terrain, $t = 150$ s. (g) Flat terrain, $t = 180$ s. (h) Gorge terrain, $t = 180$ s. (i) Flat terrain, $t = 210$ s. (j) Gorge terrain, $t = 210$ s. (k) Flat terrain, $t = 240$ s. (l) Gorge terrain, $t = 240$ s.

(about $t = 92$ s), the curves of wind attack angle of the two terrains intersect for the first time, but the values of wind attack angle at the typical monitoring points in the gorge terrain are much larger than those in the flat terrain in most time. In addition, the farther away from the midspan point, the greater the differences in wind attack angles between the two corresponding points, such as the period before 92 s (before the first intersection of the curves) and the period between 92 and 160 s (between the first and second intersections of the curves). The reason of the above phenomena relates to the differences of heights from the monitoring points to the ground between the flat and gorge

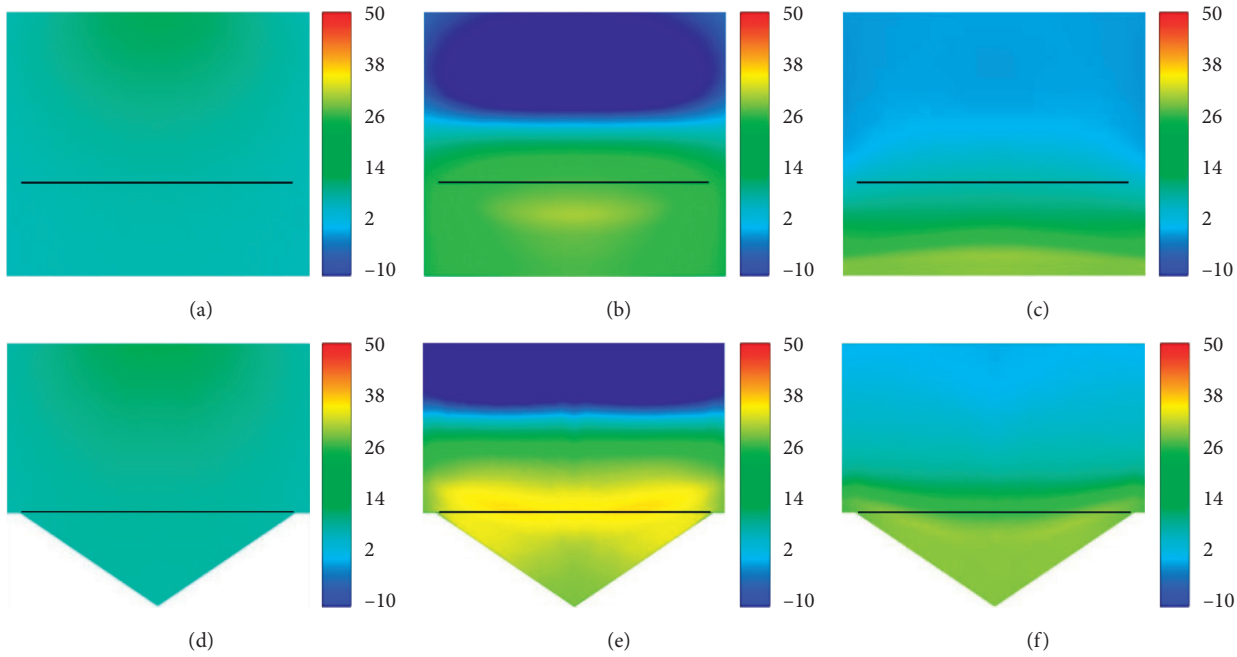

Figure 9: Contour of wind speeds in the cross section of flat and gorge terrains at the three typical time. (a) Flat terrain, $t = 50$ s. (b) Flat terrain, $t = 100$ s. (c) Flat terrain, $t = 150$ s. (d) Gorge terrain, $t = 50$ s. (e) Gorge terrain, $t = 100$ s. (f) Gorge terrain, $t = 150$ s.

terrains, and the flow is lifted by the slopes on both sides of the gorge terrain.

3.2.2. Distributions of Vertical Profile of the Wind Attack Angle. For the three typical times of $t = 50$ s, $t = 100$ s, and $t = 150$ s, the distributions of vertical profile of wind attack angle at the midspan point, 3/4 span point, and the left bridge tower in flat and gorge terrains are shown in Figure 14. Overall, most profiles of wind attack angle in flat and gorge terrains at different typical time are negative. Specifically, when $t = 50$ s, all the wind attack angle profiles at the three typical points in the flat terrain are negative, and their absolute values increase with the increase of the heights from the ground. For the gorge terrain, the profile of wind attack angle at the midspan point is negative, but it changes little with the increase of the heights from the ground. For the profile at the 3/4 span point and bridge tower, the wind attack angles are positive when the heights from the ground are low, but they gradually decrease to be negative with the increase of the heights from the ground. From Figure 8, when $t = 50$ s, the thunderstorm downburst is in the stage of sinking, and most wind attack angles around the girder are negative. However, due to the lifting effects of slopes on both sides of the gorge, certain wind attack angles near the ground may be positive, which turn to be negative when they are away from the ground due to the influences of the downward flow. When $t = 100$ s, the thunderstorm downburst hits or is about to hit the bridge girder, the monitoring points higher from the flat terrain are basically covered by the influences of the vortex, while those higher from the gorge terrain are less affected by the vortex (shown in Figure 8). Therefore, the absolute values of the wind attack angle profile in flat terrain are larger than those in gorge terrain at the midspan and 3/4 span, and the farther away from the ground, the more obvious the differences. The wind attack angle profiles at the bridge tower in flat and gorge terrains are both found to be positive, but the wind attack angles in gorge terrain are much larger than those in flat terrain, which reflects that the flow is significantly lifted by the gorge terrain, as shown in Figure 9(e). When $t = 150$ s, the first main vortex has spread horizontally, but the second vortex has not formed yet. At this time, the profiles of wind attack angle in the two terrains are still affected by the downward flow, and wind attack angles in the two terrains are basically negative. Concerning the wind attack angle profiles at the bridge tower, the profile in the gorge terrain is positive, while that in the flat terrain is negative with a larger absolute value, the reason of which is related to the differences in horizontal wind speeds at the bridge towers in the two terrains and the influences of the gorge terrain.

3.3. Synchronous Comparisons of the Wind Speed and Wind Attack Angle at the Girder. The wind speed and wind attack angle at the girder are the two most fundamental and important wind parameters in wind-resistance of bridges [23]. The performance of wind-resistance of bridges worsens with the increase of the wind speed and the wind attack angle (or its absolute value) at the girder. Generally, the higher the wind speed, the smaller the wind attack angle, and vice versa; when the wind speed is smaller, the wind attack angle is often larger, but it could not control the wind-resistance of bridges due to the smaller wind speed. The time-history curves of wind speed and wind attack angle at the girder in flat and gorge terrains under the thunderstorm downburst

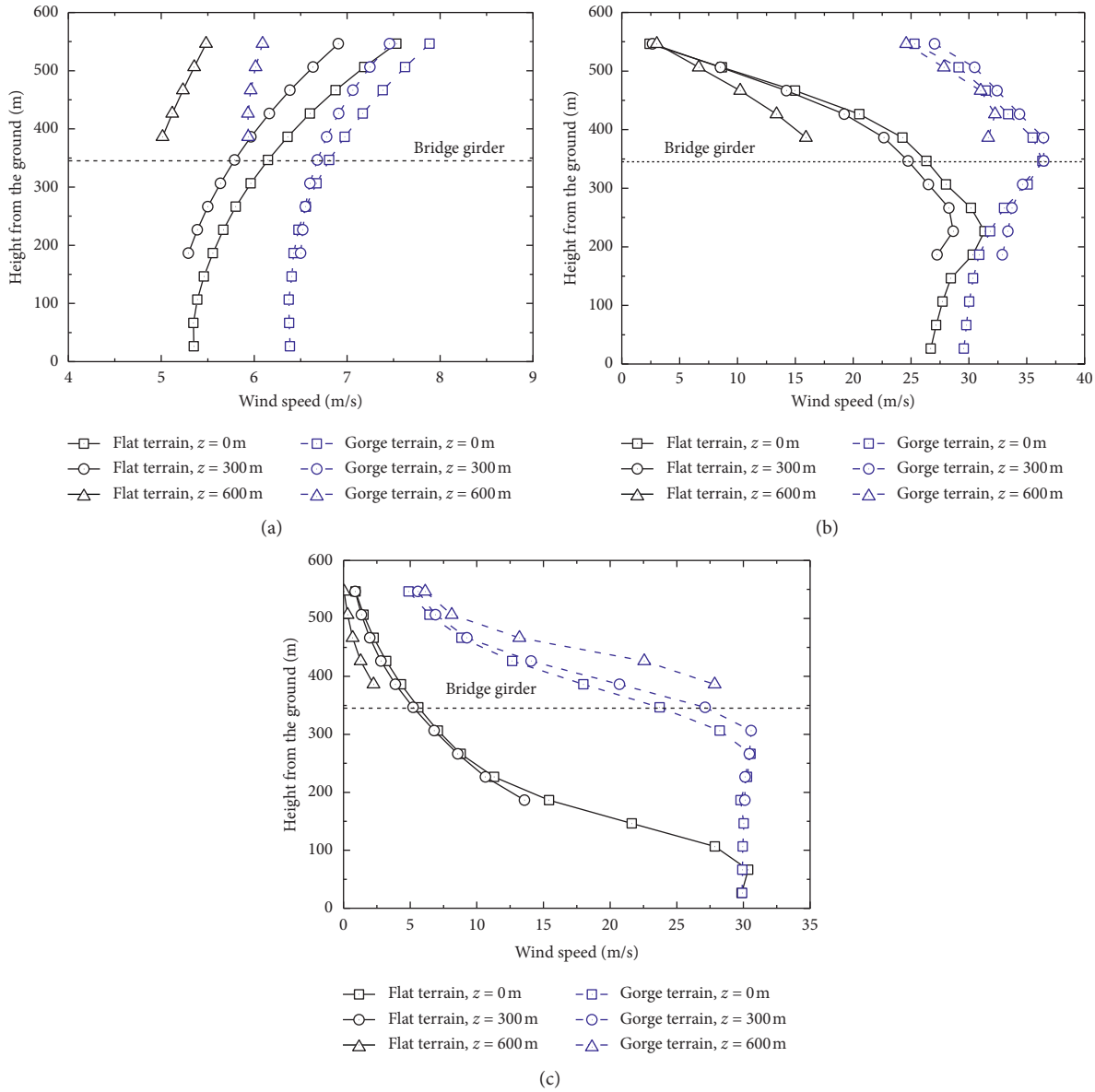

Figure 10: Distributions of vertical profile of horizontal wind speed in flat and gorge terrains at the three typical time. (a) $t = 50$ s. (b) $t = 100$ s. (c) $t = 150$ s.

are shown in Figures 15 and 16, respectively, to synchronously investigate the effects of the thunderstorm downburst on the wind speeds and wind attack angles at the girder in different terrains.

As shown in Figure 15, the wind speed and wind attack angle are both relatively large at the midspan point in flat terrain within about $t = 75$~130 s, of which the wind speed varies from 7.6 to 27.0 m/s, and the wind attack angle varies from −1.7 to −70.3°. Subsequently, although the absolute values of the wind attack angle reach nearly 90° such as at $t = 168$ s and $t = 190$ s, the corresponding wind speed is very small, which thus cannot control the wind-resistance of the bridge. Meanwhile, in the gorge terrain, the wind speed varies from 22.2 m/s to 37.8 m/s, and the wind attack angle varies from 4.1° to −25.1° from $t = 75$ s to 145 s at the midspan point. Hereafter, the wind speeds and wind attack angles have remained at a relatively high level, with the wind speed basically above 20 m/s and the wind attack angle ranging from −10.4° to −25.8°, as shown in Figure 16. Since the corresponding relationships between the wind speed and wind attack angle at other monitoring points along the girder in flat and gorge terrains are generally similar to those at the midspan point, they are not repeated here. As shown in the analysis above, the wind speed and wind attack angle (or their absolute values) at the girder in the flat terrain are large within about $t = 75$~130 s, indicating the thunderstorm downburst may exert significant effects on the bridge in this period. Similarly, the main girder in the gorge terrain may be significantly affected by the thunderstorm downburst from $t = 75$ s to 145 s. In

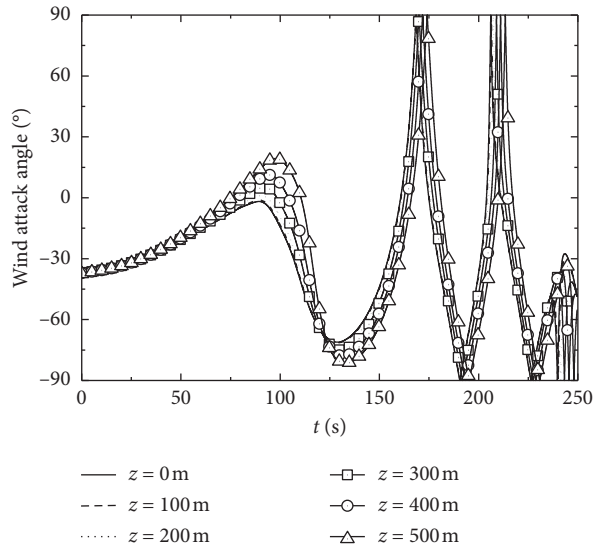

Figure 11: Time-history curves of wind attack angle in the flat terrain.

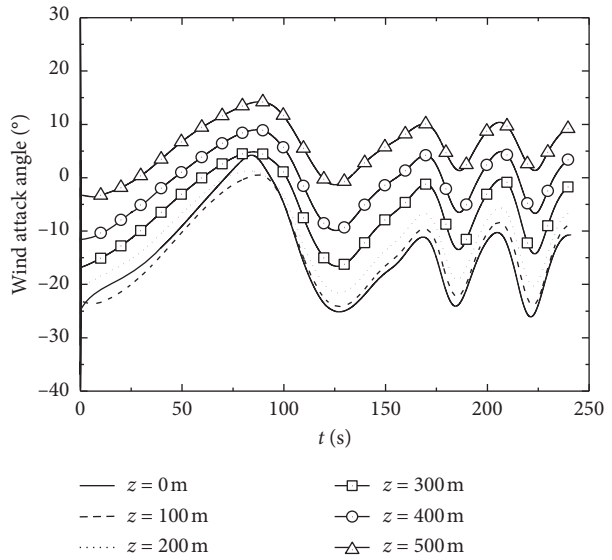

Figure 12: Time-history curves of wind attack angle in the gorge terrain.

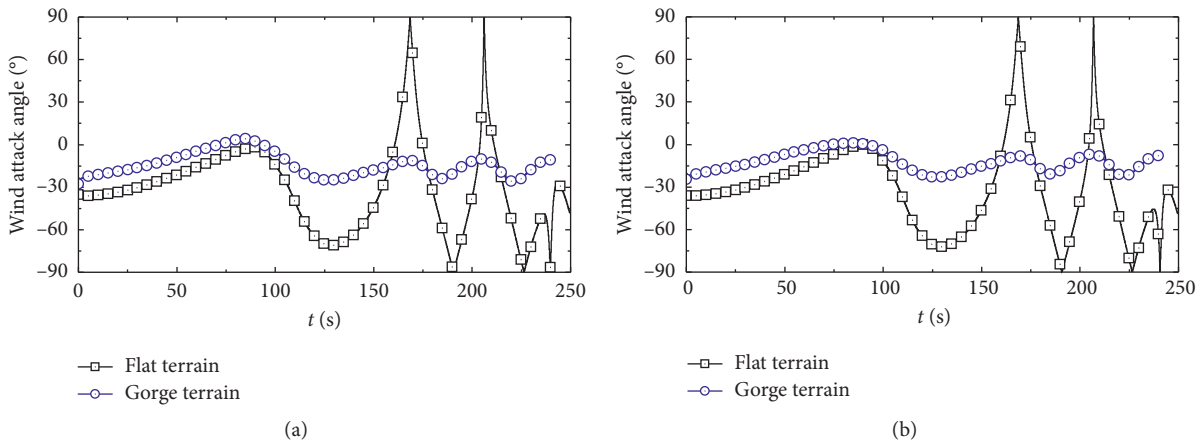

Figure 13: Continued.

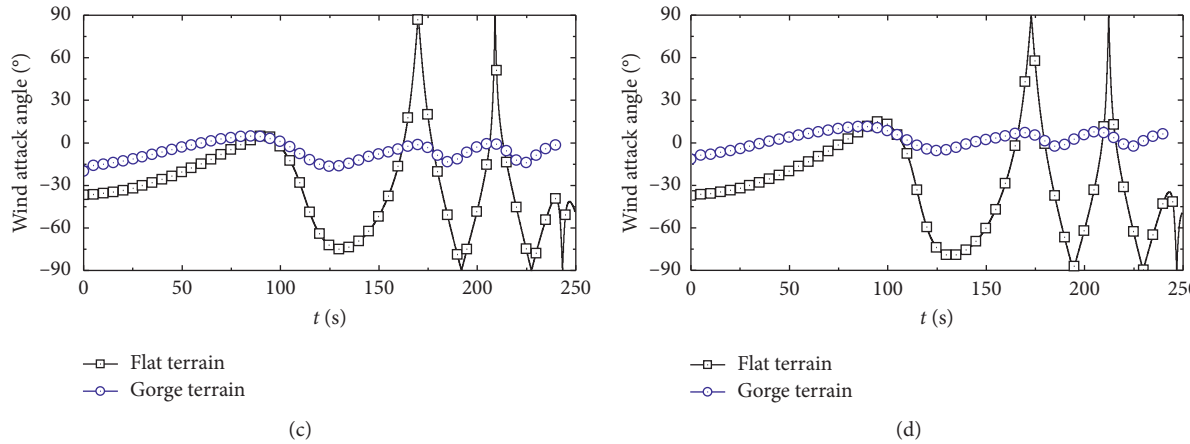

Figure 13: Comparisons between the time-history curves of wind attack angle in the flat and gorge terrains. (a) z = 0 m. (b) z = 150 m. (c) z = 300 m. (d) z = 450 m.

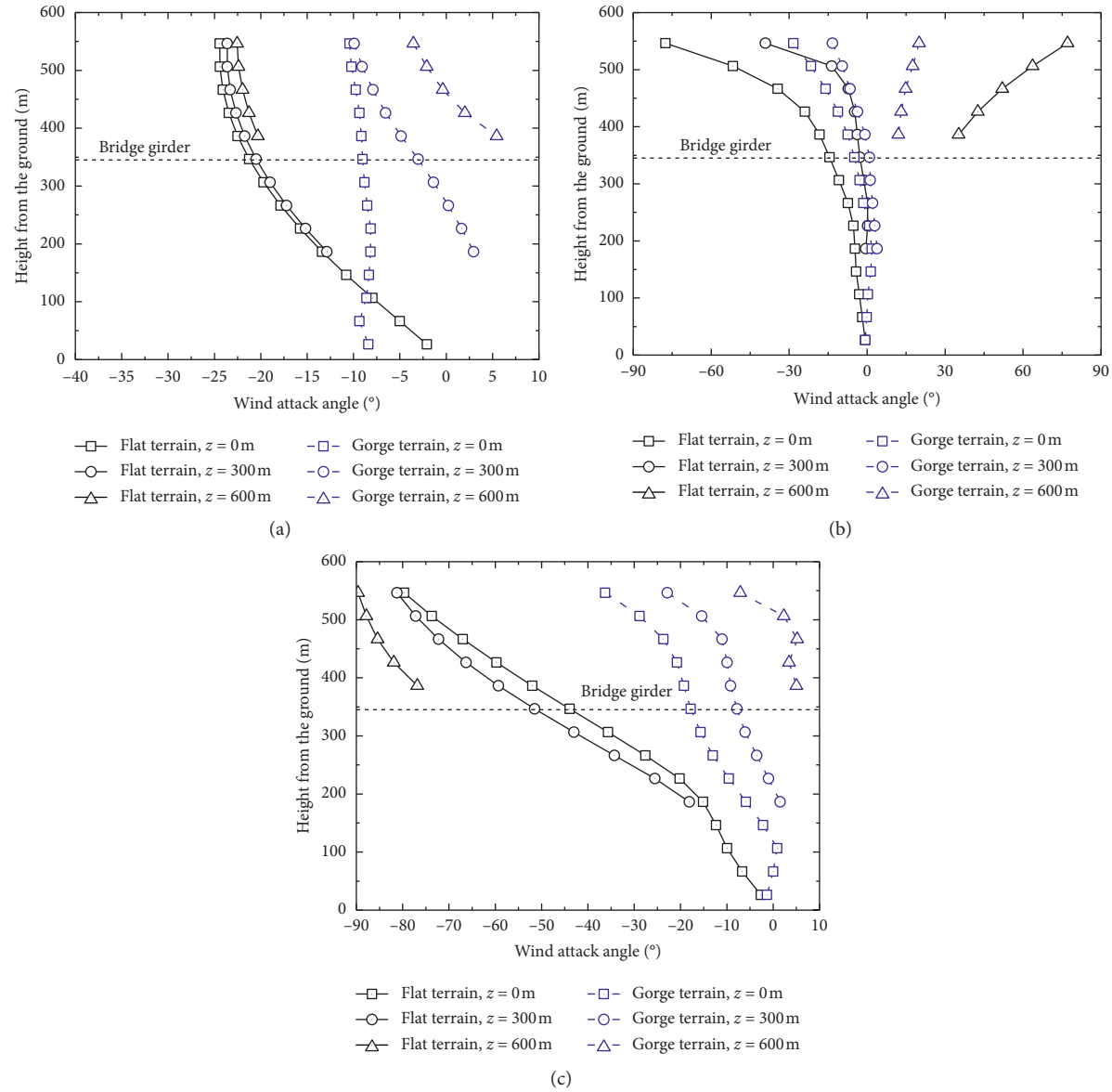

Figure 14: Distributions of vertical profile of wind attack angle in flat and gorge terrains at the three typical time. (a) $t = 50$ s. (b) $t = 100$ s. (c) $t = 150$ s.

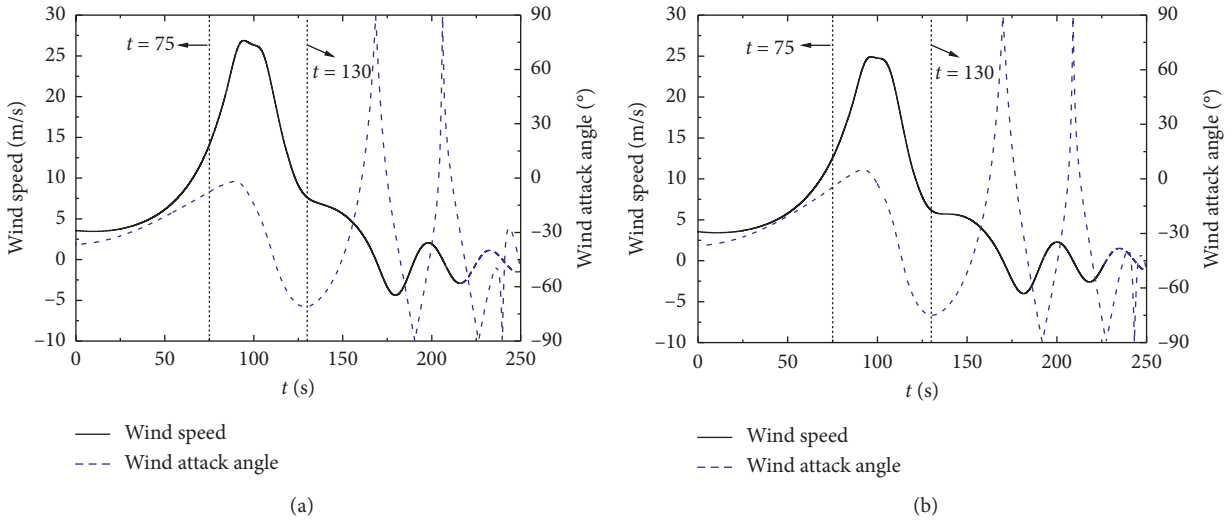

Figure 15: Synchronous comparisons of time-history curves of wind speed and wind attack angle in the flat terrain. (a) The midspan point. (b) The 1/4 span point.

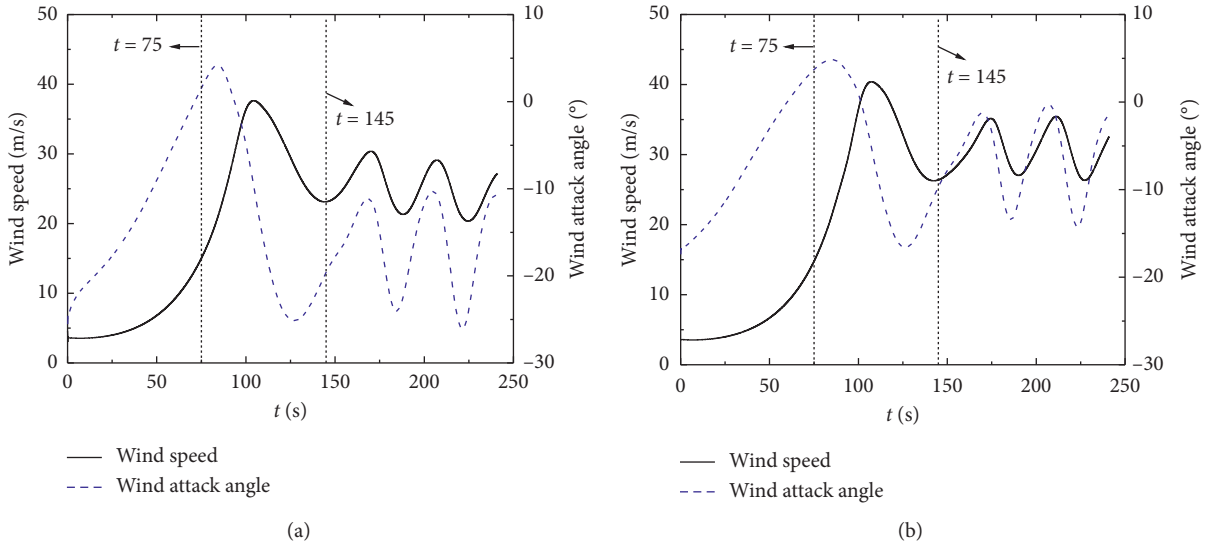

Figure 16: Synchronous comparisons of time-history curves of wind speed and wind attack angle in the gorge terrain. (a) The midspan point. (b) The 1/4 span point.

addition, the responses of the girder after $t = 145$ s should also be paid full attention, since the wind speed and wind attack angle (or their absolute values) at the girder are still large in the following time.

4. Conclusions

The characteristics of wind field in flat and gorge terrains under the thunderstorm downburst are investigated by numerical simulations in this paper, and the distributions of horizontal wind speed and wind attack angle in the two different terrains are analyzed. The conclusions reached are as follows:

(1) The radial and vertical profiles of horizontal wind speed under the thunderstorm downburst over the flat terrain are investigated based on the SST k-ω turbulence model, combined with the impinging jet technology. The accuracy of the numerical simulation results in this paper is verified through comparison with the previous studies, which validates the rationality and feasibility of the present mesh scheme and other settings, providing a basis for further numerical simulation research.

(2) Under the effects of the thunderstorm downburst, the wind speeds are relatively maximum at the midspan point of the girder in the flat terrain, and the farther away from the midspan point, the smaller the values of the wind speed. However, the wind speeds are relatively minimum at the midspan point of the girder in the gorge terrain, and the farther

away from the midspan point, the larger the values of wind speed. The wind speeds at each typical monitoring point are basically consistent in the two terrains before the thunderstorm downburst hits the bridge site, after which, the wind speeds at each point over the gorge terrain are much higher than those in the flat terrain, and its peak of wind speed is later than that in flat terrain.

(3) When $t = 100$ s, the wind speed reaches its maximum at the 40 m above the bridge girder in gorge terrain, while the maximum wind speed is found 120 m below the bridge girder in flat terrain, the reason of which relates to the relative position between the main vortex and girder in different terrains.

(4) Under the effects of the thunderstorm downburst, most wind attack angles are negative at the monitoring points in the flat terrain, but the farther away from the midspan point, the larger the wind attack angles. The wind attack angles at these monitoring points in gorge terrain share the similar variation trend to those in flat terrain. However, the wind attack angles at the monitoring points farther away from the midspan point gradually turn to be positive. Besides, the wind attack angles at the typical monitoring points in gorge terrain are generally larger than those in flat terrain, with a much smaller fluctuation range.

(5) Both the wind speeds and wind attack angles (or their absolute values) at the girder in the flat terrain are large within about $t = 75$~130 s, indicating that significant effects may be exerted by the thunderstorm downburst on the bridge. Similarly, the girder in the gorge terrain may be significantly affected by the thunderstorm downburst from $t = 75$ s to 145 s. Since the wind speeds and wind attack angles (or their absolute values) of the girder are still large after $t = 145$ s, full attention should be paid to the effects of thunderstorm downburst on the bridge during this period.

In the present study, a simple flat terrain and a simple gorge terrain were considered to explore the general trends and mechanism of wind field characteristics at the bridge site under the thunderstorm downbursts. In the future, the wind field characteristics at actual bridge sites in the actual gorge terrains together with the moving thunderstorm downbursts will be further considered.

Data Availability

The data used to support the findings of this study are available from the corresponding author upon request.

Conflicts of Interest

The authors declare that there are no conflicts of interest regarding the publication of this paper.

Acknowledgments

This study received funds from the National Natural Science Foundation of China (grant nos. 51878080 and 51822803) and the Hunan Provincial Natural Science Foundation of China (grant nos. 2020JJ3035 and 2018JJ3538).

References

[1] T. T. Fujita, "Downburst: meteorological features and wind filed characteristics," *Journal of Wind Engineering and Industrial Aerodynamics*, vol. 36, no. 1, pp. 75–86, 1900.

[2] T. T. Fujita, *Andrews AFB Microburst, SMRP Research Paper 205*, University of Chicago, Chicago, Illinois, USA, 1985.

[3] F. H. Proctor, "Numerical simulations of an isolated microburst. Part I: dynamics and structure," *Journal of the Atmospheric Sciences*, vol. 45, no. 21, pp. 3137–3160, 1988.

[4] F. T. Lombardo, "Improved extreme wind speed estimation for wind engineering applications," *Journal of Wind Engineering and Industrial Aerodynamics*, vol. 104-106, pp. 278–284, 2012.

[5] A. Elawady, H. Aboshosha, A. El Damatty, G. Bitsuamlak, H. Hangan, and A. Elatar, "Aero-elastic *testing* of multi-spanned transmission line subjected to downbursts," *Journal of Wind Engineering and Industrial Aerodynamics*, vol. 169, pp. 194–216, 2017.

[6] T. T. Fujita, "Manual of downburst identification for project NIMROD," *SMRP Research Paper*, vol. 156, pp. 104–112, 1978.

[7] R. M. Wakimoto, "The life cycle of thunderstorm gust fronts as viewed with Doppler radar and rawinsonde data," *Monthly Weather Review*, vol. 110, no. 8, pp. 1060–1082, 1982.

[8] M. R. Hjelmfelt, "Structure and life cycle of microburst outflows observed in Colorado," *Journal of Applied Meteorology*, vol. 27, no. 8, pp. 900–927, 1988.

[9] S. Zhang, Q. S. Yang, G. Solari, B. Li, and G. Q. Huang, "Characteristics of thunderstorm outflows in Beijing urban area," *Journal of Wind Engineering and Industrial Aerodynamics*, vol. 195, Article ID 104001, 2019.

[10] G. S. Wood, K. C. S. Kwok, N. A. Motteram, and D. F. Fletcher, "Physical and numerical modelling of thunderstorm downbursts," *Journal of Wind Engineering and Industrial Aerodynamics*, vol. 89, no. 6, pp. 535–552, 2001.

[11] W. E. Lin and E. Savory, "Physical modelling of a downdraft outflow with a slot jet," *Wind and Structures An International Journal*, vol. 13, no. 5, pp. 385–412, 2010.

[12] M. T. Chay and C. W. Letchford, "Pressure distributions on a cube in a simulated thunderstorm downburst-Part A: stationary downburst observations," *Journal of Wind Engineering and Industrial Aerodynamics*, vol. 90, no. 7, pp. 711–732, 2002.

[13] C. Li, Q. S. Li, Y. Q. Xiao, and J. P. Ou, "A revised empirical model and CFD simulations for 3D axisymmetric steady-state flows of downbursts and impinging jets," *Journal of Wind Engineering and Industrial Aerodynamics*, vol. 102, pp. 48–60, 2012.

[14] L. Chen and C. W. Letchford, "Numerical simulation of extreme winds from thunderstorm downbursts," *Journal of Wind Engineering and Industrial Aerodynamics*, vol. 95, no. 9-11, pp. 977–990, 2007.

[15] Z. W. Liu, Y. L. Chen, Y. B. Xin, and Z. Q. Chen, "Numerical simulation on steady wind field characteristics of downburst based on atmosphere boundary layer wind tunnel," *Journal of Hunan University*, vol. 47, no. 7, pp. 10–20, 2020, in Chinese.

[16] M. S. Mason, G. S. Wood, and D. F. Fletcher, "Numerical investigation of the influence of topography on simulated downburst wind fields," *Journal of Wind Engineering and Industrial Aerodynamics*, vol. 98, no. 1, pp. 21–33, 2010.

[17] E.-S. Abd-Elaal, J. E. Mills, and X. Ma, "Numerical simulation of downburst wind flow over real topography," *Journal of Wind Engineering and Industrial Aerodynamics*, vol. 172, pp. 85–95, 2018.

[18] G. Huang, Y. Jiang, L. Peng, G. Solari, H. Liao, and M. Li, "Characteristics of intense winds in mountain area based on field measurement: focusing on thunderstorm winds," *Journal of Wind Engineering and Industrial Aerodynamics*, vol. 190, pp. 166–182, 2019.

[19] *Wind-resistant Design Specification for Highway Bridges*, Ministry of Transport of the People's Republic of China, Beijing, China, 2018, in Chinese.

[20] J. Hao and T. Wu, "Downburst-induced transient response of a long-span bridge: a CFD-CSD-based hybrid approach," *Journal of Wind Engineering and Industrial Aerodynamics*, vol. 179, pp. 273–286, 2018.

[21] M. S. Mason, G. S. Wood, and D. F. Fletcher, "Impinging jet simulation of stationary downburst flow over topography," *Wind and Structures*, vol. 10, no. 5, pp. 437–462, 2007.

[22] P. Hu, Y. Han, G. J. Xu, Y. L. Li, and F. R. Xue, "Numerical simulation of wind fields at the bridge site in mountain-gorge terrain considering an updated curved boundary transition section," *Journal of Aerospace Engineering*, vol. 31, no. 3, Article ID 04018008, 2018.

[23] P. Hu, Y. Han, C. S. Cai, and W. Cheng, "Wind characteristics and flutter performance of a long-span suspension bridge located in a deep-cutting gorge," *Engineering Structures*, vol. 233, Article ID 111841, 2021.